Available online at www.sciencedirect.com
ScienceDirect
Journal of the European Ceramic Society 31 (2011) 1881–1888
www.elsevier.com/locate/jeurceramsoc

Microstructure and thermo-physical properties of yttria stabilized zirconia coatings with CMAS deposits

Jing Wu, Hong-bo Guo *, Yu-zhi Gao, Sheng-kai Gong

Key Laboratory of Aerospace Materials & Performance (Ministry of Education), School of Materials Science and Engineering, No. 37 Xueyuan Road, Beijing 100191, China

Received 17 January 2011; received in revised form 24 March 2011; accepted 3 April 2011
Available online 22 April 2011

Abstract

Yttria stabilized zirconia (YSZ) thermal barrier coatings (TBCs) are used to protect hot-components in aero-engines from hot gases. In this paper, the microstructure and thermo-physical and mechanical properties of plasma sprayed YSZ coatings under the condition of calcium–magnesium–alumina–silicate (CMAS) deposits were investigated. Si and Ca in the CMAS rapidly penetrated the coating at 1250 °C and accelerated sintering of the coating. At the interface between the CMAS and YSZ coating, the YSZ coating was partially dissolved in the CMAS, inducing the phase transformation from tetragonal phase to monoclinic phase. Also, the porosity of the coating was reduced from ∼25% to 5%. As a result, the thermal diffusivity at 1200 °C increased from 0.3 mm^2/s to 0.7 mm^2/s, suggesting a significant degradation in the thermal barrier effect. Also, the coating showed a ∼40% increase in the microhardness. The degradation mechanism of TBC induced by CMAS was discussed.

Keywords: Thermal barrier coatings (TBCs); Calcium–magnesium–alumina–silicate (CMAS); Microstructure; Thermal diffusivity; Microhardness

1. Introduction

Thermal barrier coatings (TBCs) have been widely employed to improve the durability of hot section components in gas turbine engines.[1–4] Because of the demanding extreme operating conditions, TBCs possess one of the most complex structures among the widely available coatings which are used to protect structural materials from various environments. TBCs are multilayered systems consisting of a ceramic topcoat for thermal insulation, a thermally grown oxide (TGO) scale, predominantly Al_2O_3, a metallic bond coat that provides oxidation/hot corrosion resistance, and a superalloy substrate that is the load-bearing component. The ceramic topcoat of TBCs is typically made of zirconia partially stabilized with yttria (YSZ) for its low thermal conductivity and high thermal expansion coefficient.[5]

With the ever increasing demand to increase the turbine inlet temperature (TIT) for improved engine efficiency, a prime reliability TBCs system to effectively protect the hot section turbine components has been a critical requirement for gas turbine engines. Extensive efforts have been made to identify the failure mechanisms of the TBCs to increase the durability and reliability of TBCs.[6–9] Among the various life-limiting factors, one key durability issue of TBCs is their resistance to environmental degradation due to molten deposits arising from the aggressive combustion environment as well as from air-ingested foreign particles, commonly known as calcium–magnesium–alumina–silicate (CMAS, $CaO–MgO–Al_2O_3–SiO_2$) which refers to the main chemical components of Ca, Mg, Al, and Si.[10–13] The CMAS melts are produced when siliceous minerals (dust, sand, volcanic ash, and runway debris) are ingested with the intake air and deposited on the hot surface of the components. Below the melting point, these deposits cause erosive wear, blockage of cooling holes and local spallation. When operated at high temperature, these deposits melt and adhere to the coating surface. They rapidly penetrate into the whole coating through the open pores of the coating, and during cooling stage, these deposits crystallize and cause spallation of the coating because of the thermal expansion mismatch between the CMAS and the coating. CMAS damage to TBCs has been investigated in detail by Mercer et al.,[14] Krämer et al.,[15] Li et al.,[16] Chen,[17] and Aygun et al.[18] Some efforts have been made to improve the resistance of TBCs to high-temperature attack by glassy deposits.[19,20]

* Corresponding author. Tel.: +86 10 8231 7117; fax: +86 10 8233 8200.
E-mail address: guo.hongbo@buaa.edu.cn (H.-b. Guo).

0955-2219/$ – see front matter © 2011 Elsevier Ltd. All rights reserved.
doi:10.1016/j.jeurceramsoc.2011.04.006

Table 1
Processing parameters for plasma spraying of YSZ coatings (*D*: spray distance; *F*: feed rate; *V*: transverse speed of plasma gun).

Power (kW)	*D* (mm)	Ar (slpm)	H_2 (slpm)	*F* (g/min)	*V* (mm/s)
37.5	120	80	16	40	500

The objective of this study is to investigate the microstructure evolution of plasma sprayed YSZ coatings under the simulate CMAS condition and understand the effect of CMAS deposits on the thermo-physical and mechanical properties of the coatings. Also, the CMAS degradation mechanism of the YSZ TBC is also discussed.

2. Experimental procedures

2.1. Preparation of the simulated CMAS coating

Ni-based superalloy K3 was used as the substrate materials for TBCs. YSZ coatings were prepared by Metco 7M atmospheric plasma spray facility with 9 MB spray pistol and Metco 4MP-dual type feedstock system. The 7.8 wt.% Y_2O_3 and 2.6 wt.% HfO_2 stabilized zirconia powder feedstock was used for spraying the YSZ coatings, which mostly comprised tetragonal phase with the content of more than 94%. Free-standing YSZ coating specimens were produced by removing the coatings from the substrates using hydrochloric acid. The processing parameters for spraying the YSZ coating are listed in Table 1. The choice of spray parameters were based on the first author's previous work.[21]

A laboratory synthesized CMAS with chemical composition of $22CaO–19MgO–14AlO_{1.5}–45SiO_2$ in mole percent was used in this study. The chemical composition of CMAS was determined based on the chemical composition of the deposits on vane blades in aircraft engines after hundreds times of flight service. The CMAS was prepared by mechanically milling the mixtures of CaO, MgO, Al_2O_3 and SiO_2 at room temperature for 24 h. The CMAS powders were deposited onto the YSZ coating specimens by plasma spraying at a concentration of 20 mg/cm^2. The feedstock morphology of the simulated CMAS was shown in Fig. 1. The average size of the powder was ∼150 μm. The simulated CMAS particles were agglomerated to enhance the powder flow ability. After agglomeration, the composition of the CMAS deposits showed a little variation. The content of Si decreased, while the contents of Ca and Al increased, as shown in Table 2, possibly due to the loss of SiO_2 during ball milling.

Table 2
Chemical composition of CMAS deposits on the YSZ free-standing coating samples (mol%).

SiO_2	CaO	MgO	$AlO_{1.5}$
30.44	28.15	18.85	22.56

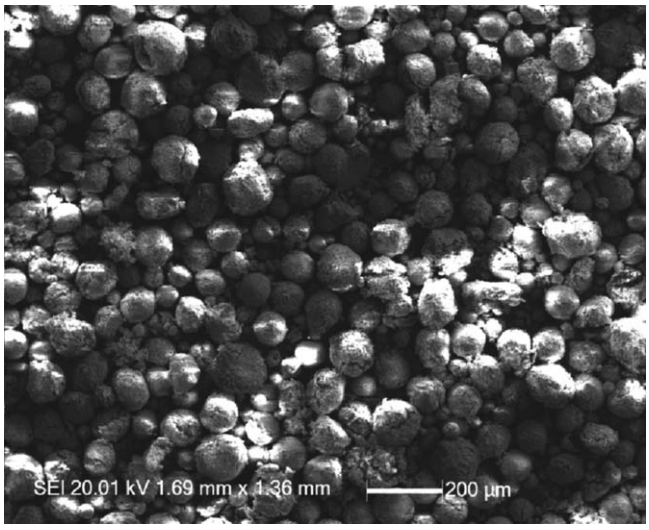

Fig. 1. Morphology of the simulated CMAS powders for spraying.

2.2. Heat treatment

Heat treatment of free-standing coating specimens with CMAS deposits was performed in a muffle furnace. The specimens were heated in the furnace to 1250 °C and held at this temperature for 4 h, 8 h, 16 h, 24 h and 48 h, respectively. Both the heating and cooling rates were kept at 6 °C/min. The temperature for heat-treatment was chosen based on the CMAS deposits melting temperature reported in literature.[15]

2.3. Microstructure characterization

The microstructure of the YSZ coating was characterized by a QUANTA 144 600 scanning electron microscopy (SEM). The porosity of the free-standing coating was determined by a mercury porosimetry (Micromeritics Autopore II, Shimadzu, Kyoto, 149 Japan). Before the porosity measurement, all the surfaces of the specimens were finely polished in order to eliminate the effect of surface roughness on the porosity measurements. As Raman spectroscopy is particularly sensitive to zirconia polymorphs,[22] Raman spectra were measured on RM2000 Raman spectroscopy (Renishaw Company, UK) to identify the phase change of YSZ coatings caused by CMAS attack at high temperature. The crucial parameters were used as follows: laser wavelength: 632.8 nm; Raman shift scope: 100–4000 cm^{-1}; microscope: ≥1 μm; wave resolution of spectrum: 1 cm^{-1}. Raman spectroscopy was used to analyze the phases of YSZ coating adjacent to the CMAS deposit. Along the white line, every 5 μm distance, the phase of YSZ was characterized.

2.4. Thermo-physical properties

Free-standing YSZ coating specimens were produced by removing the coatings from the substrates using hydrochloric acid. The diffusivity of the free-standing YSZ coatings was determined by laser flash technique. Thermal diffusivity

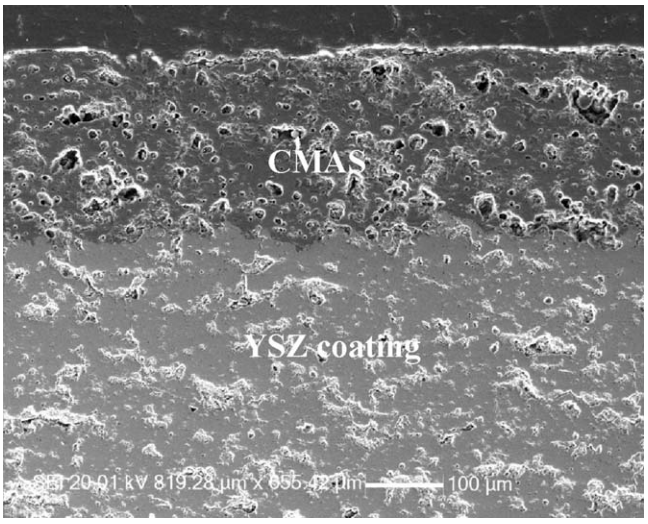

Fig. 2. SEM micrograph of cross-section of the YSZ coating with CMAS deposit.

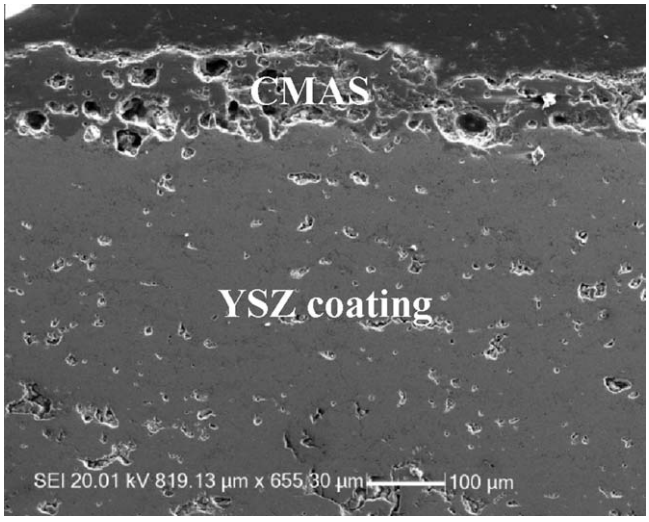

Fig. 3. SEM micrograph of cross-section of the YSZ coating with CMAS after 4 h heat-treatment at 1250 °C.

$\alpha(T)$ measurements were conducted using a laser device (LFA 427/71/G, Netzsch) on disk-shaped specimens of 12.6 mm in diameter and 1 mm in height. During measurement, the specimens were heated from room temperature up to 1200 °C. The thermal diffusivity data were recorded every 100 °C. Before the measurements, the specimen surfaces were coated with a thin film of carbon to increase the absorption of laser pulses.

Porosity size distributions in the free-standing YSZ coating specimens were determined by a mercury porosimetry (Micromeritics Autopore II, Shimadzu, Kyoto, Japan). In order to avoid the effect of surface roughness, the surfaces of the specimens were finely polished before measurement. The maximum pressure applied during measurement was 400 MPa, corresponding to a pore diameter of 4 nm. The volume shrinkages of the specimens at 1250 °C for 10 h were determined using a high-temperature dilatometer (Netzsch DIL 402E, Germany) on specimens of 25 mm in length and 5 mm in both width and height.

2.5. Microhardness

The Vickers hardness of the YSZ coatings subjected to CMAS attack was measured in their cross sections using a microhardness indenter. A load of 50 g was applied onto the specimens during the measurement, with a loading time of 10 s.

3. Results

The microstructure of the as-sprayed CMAS deposits is shown in Fig. 2. The CMAS deposits were loose and porosity, very similar to the morphology of the YSZ coating. There were mainly two kinds of pores in the CMAS deposit. The coarse pores mainly resulted from the semi-molten feedstock, and the finer pores were the typical feature of APS coating. The deposits thickness was ~200 μm.

The YSZ coating samples with the CMAS deposits were heat-treated at 1250 °C to allow CMAS to infiltrate into the YSZ coating. After 4 h heat-treatment, the CMAS deposit thickness decreased to ~100 μm and some coarsen bubbles were formed in the deposits (Fig. 3). It can be inferred that the CMAS melted at 1250 °C and infiltrated into the YSZ coating. The fine pores in the YSZ coating were filled with some dark phases. The dark phases were mainly consisting of Si and small amount of Ca by EDS. Correspondingly, the contents of Si and Ca in the CMAS deposits decreased to ~5 at.% and less than 1 at.%. On the other hand, the YSZ coating became denser since the large porosity in the as-sprayed coating obviously decreased after heat-treatment.

Besides the CMAS infiltration into the YSZ coating, there is a loose zone between the YSZ and the CMAS deposits, where fine spherical particles were observed, as shown in Fig. 4a. The thickness of this zone was about 15 μm. By EDS, this zone was still made of YSZ. From the Raman result, in the zone very closed to the CMAS deposit, there was m-phase YSZ peak at ~200 cm^{-1} Raman shift, as shown in Fig. 4b. In this zone, t-phase YSZ was transformed to m-phase.

After 8 h (Fig. 5a) heat-treatment, the depth for the interaction zone between the CMAS and YSZ coating is ~20 μm and increased to ~30 μm after 16 h heat-treatment (Fig. 5b). However, the interaction zone did not show apparent increase in the depth after longer times as shown in Fig. 5c and d.

As the CMAS began to melt at 1250 °C, the glassy CMAS rapidly infiltrated into the YSZ coating, as shown in Fig. 6. After 8 h heat-treatment, the infiltration thickness of CMAS was ~400 μm, and the infiltrated zone in the YSZ was apparently denser than the un-affected zone, as shown in Fig. 6a. The infiltration thickness increased to ~600 μm after 16 h heat-treatment (Fig. 6b) and after 36 h, CMAS almost penetrated into the whole coating (Fig. 6c and d).

The porosity distribution of the coatings revealed a typical bimodal distribution of small and large pore sizes, as shown in

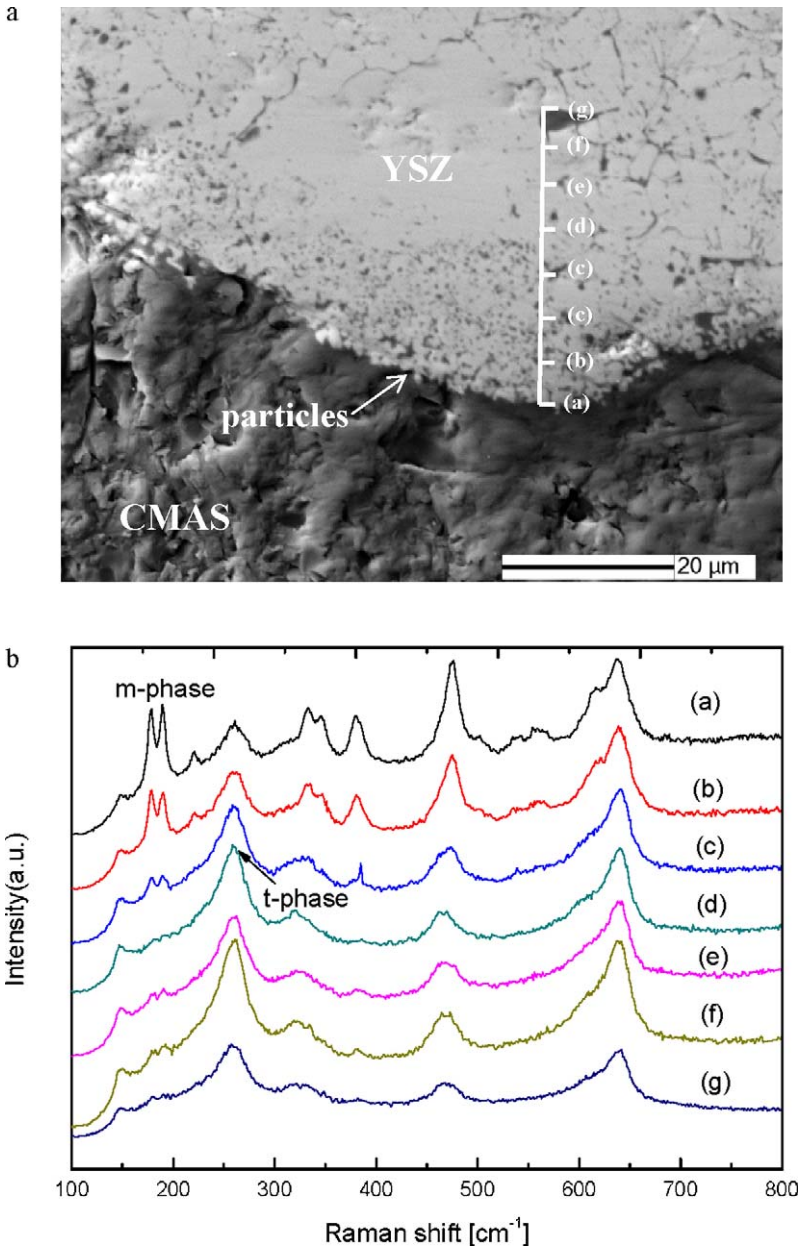

Fig. 4. (a) Micrograph of the interaction zone of CMAS deposit and YSZ coating after 4 h heat-treatment at 1250 °C, and (b) Raman spectra obtained from the positions marked in (a).

Fig. 7. Before heat-treatment, the free-standing coating had a porosity of ~25%, while the porosity reduced to ~22% after 10 h heat treatment. However, for the YSZ coating with CMAS deposits, the porosity was only 5%, which shown a significant reduction. It can be supposed that for the TBC with deep CMAS penetration, the thermal barrier function would be severely compromised. This was confirmed by the thermal diffusivity measurement results as shown in Fig. 8. The as-sprayed coating had a thermal diffusivity of ~0.3 mm^2/s at 1200 °C. At the same temperature, the thermal diffusivity for the coating subjected to 10 h heat-treatment increased to ~0.4 mm^2/s. Compared to it, the thermal diffusivity for the coating subjected to 10 h CMAS attack increased further to ~0.7 mm^2/s. The thermal diffusivity for the coating with CMAS penetration was nearly 70% higher than that of the coating without CMAS penetration at the same temperature with 10 h heat-treatment.

Sintering behaviors of the free-standing YSZ coatings at 1250 °C were investigated. As shown in Fig. 9, the shrinkage of the only YSZ coating and the coating with CMAS penetration were compared. In the case of the only YSZ coating, a total shrinkage (dL/dL_0) of ~0.22% was observed after 10 h heat-treatment. For the coating with CMAS infiltration, the shrinkage is about 1.1%. This implies that CMAS infiltration could contribute to faster sintering of TBC.

Fig. 10 displayed the microhardness of the YSZ coatings subjected to CMAS attack at 1250 °C. The coating before heat-treatment had a microhardness of 6–8 GPa, while the microhardness increased to 10–13 GPa after 50 h heat-treatment.

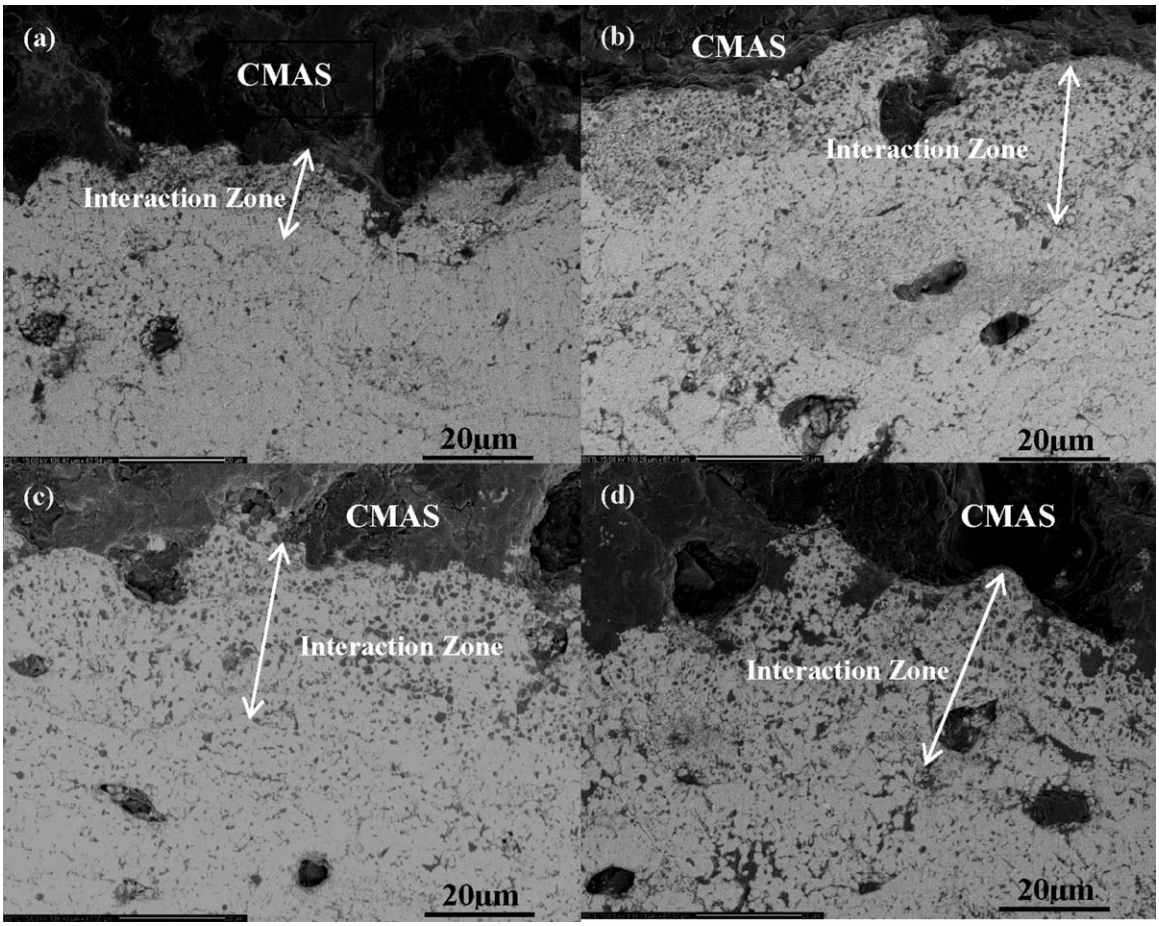

Fig. 5. Back scatter images of cross-sections of YSZ coatings with CMAS deposits after heat-treatment at 1250 °C for different time: (a) 8 h, (b) 16 h, (c) 24 h, and (d) 48 h.

CMAS attack together with sintering led to an improvement of more than 25% in the microhardness.

4. Discussion

4.1. Effect of CMAS deposits on YSZ coating microstructure

In the present observation, CMAS deposits melted at 1250 °C and rapidly infiltrated into YSZ coating. In the interface between CMAS deposits and YSZ coating, the original t phase YSZ was dissolved and reprecipitated into loose particles of m-phase, as shown in Fig. 5. The infiltration parts of CMAS deposits were mainly Si and a little Ca.

The mechanism by which the YSZ phase changes happen in the interface is still under investigation. One possible assumption is that the ZrO_2 grains are dissolved in the molten CMAS glass and reprecipitate in globular forms.[23] Globular nature of the ZrO_2 grains provides a strong indication for diffusion-controlled dissolution reprecipitation. The transformation of t-ZrO_2 to m-ZrO_2 appears to take place during dissolution re-precipitation.[24] Another assumption is that a lower Y content, which is dissolved in CMAS, leads to the instability YSZ.[15]

The interaction zones between the CMAS deposits and TBC didn't show apparent increase in the depth after 16 h. The reasons for this maybe that the Si and Ca elements in the CMAS quickly infiltrated into the YSZ coating once the melting temperature approached. As a result, the contents of Si and Ca in the CMAS decreased. With the time, Si and Ca in the CMAS became less and less. Consequently, the interaction between CMAS and YSZ was significantly decelerated.

The time, t, needed for the CMAS glass to penetrate the porous TBC can be roughly calculated based on the following equation[18]:

$$t \sim \left[\frac{k_t}{8D_C}\left(\frac{1-\omega}{\omega}\right)^2 L^2\right]\frac{\eta}{\sigma_{LV}}$$

where η is the CMAS glass viscosity, σ_{LV} the glass surface tension, k_t the tortuosity of TBC pores, ω the porosity open to flow, and D_c the capillary diameter. The CMAS glass viscosity η is referred to be ~49 Pa,[25] while $\sigma_{LV} \sim 0.4\,Jm^{-2}$, $k_t \sim 10$, and $D_c \sim 1\,\mu m$[18], respectively. The open porosity ω of the YSZ coating in the present work is measured to be ~0.25. According to the above equation, the time for CMAS penetrating into the 400 μm thickness YSZ coating is nearly 4 h, and the time for CMAS penetrating into the 1 mm thickness coating nearly 22 h. These results were well consistent with the experiment results as shown in Fig. 6.

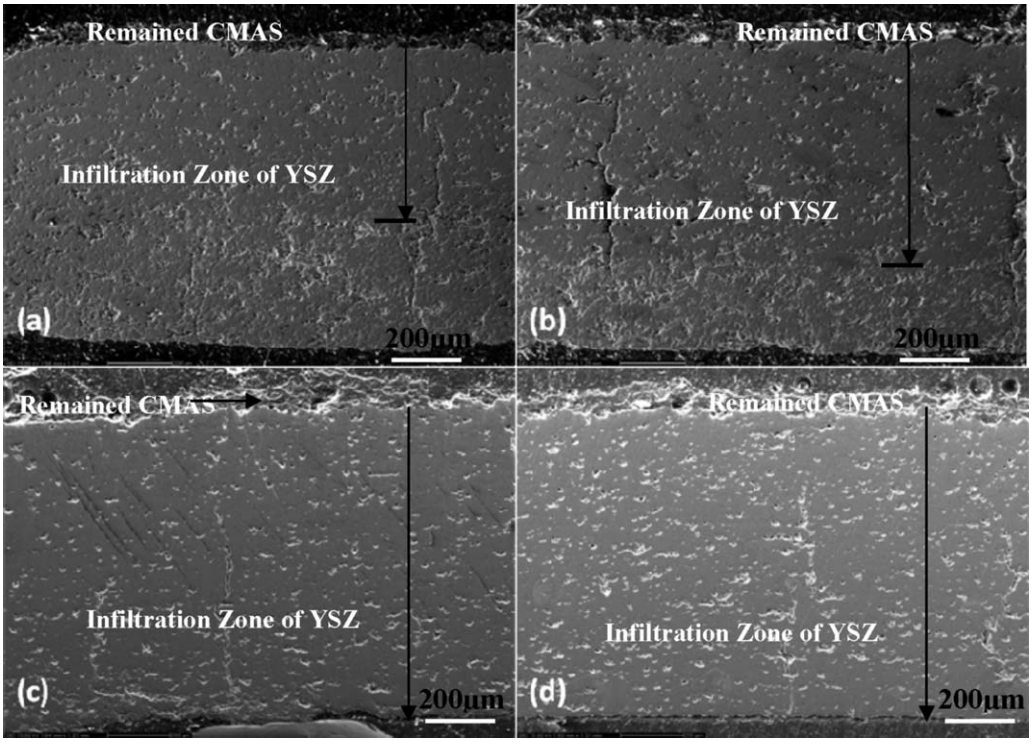

Fig. 6. SEM micrographs of cross-sections of the free-standing YSZ coatings with CMAS after heat-treatment at 1250 °C for diferent time: (a) 8 h, (b) 16 h, (c) 24 h and (d) 48 h.

The small pore sizes are mainly attributed to microcracks and intersplat gaps within the coating.[26–29] When the YSZ coating was held at 1250 °C, the glassy CMAS penetrated into the coating quickly and filled most of the open porosities which led to the significant reduction in porosity.

According to the shrinkage result shown in Fig. 9, CMSA deposits caused accelerated sintering of YSZ coating. As earlier mentioned, when CMAS infiltrated, there were in fact Si and Ca elements diffusing into the YSZ coating. CaO was ever used as stabilizer for zirconia and the infiltration quantity was much less than that of SiO_2, so the effect of Ca on sintering of YSZ can be ignored. Silica has a significant influence on the sintering behavior of YSZ coating, promoting sintering of the coating during high-temperature annealing. An explanation about this might be the observation of silica-rich phase at grain boundaries. These phases have a low viscosity at elevated temperatures and can promote densification by liquid-phase sintering. It has been shown that SiO_2 was detrimental to the thermal cyclic life times of YSZ coating.[30] In zirconia ceramics, SiO_2 was segregated at grain boundaries and enriched in triple points. Y_2O_3 was precipitated from YSZ grain boundaries, which led to local instability. Otherwise, SiO_2 caused the ZrO_2 super-plasticity, accelerated the sintering speed.

4.2. *Effect of CMAS deposits on thermo-physical properties of YSZ coatings*

For a TBC, pores and microcracks in the ceramic layer contribute significantly to the thermal barrier function, as they can reduce the thermal conductivity of the coating by more than a factor of two over the bulk ceramic material.[30] During high-temperature exposure, glassy CMAS easily infiltrated into the coatings by inter-connected pores and cracks, then filled the pores and cracks. On the other hand, as discussed above, accelerated sintering of YSZ coating occurred due to CMAS infiltration. Thus, the porosity of the coating was significantly reduced, as shown in Fig. 7. As a result, the thermal diffusivity of the YSZ coating with CMAS infiltration was nearly 70% higher than that of the coating without CMAS infiltration, as shown in Fig. 8.

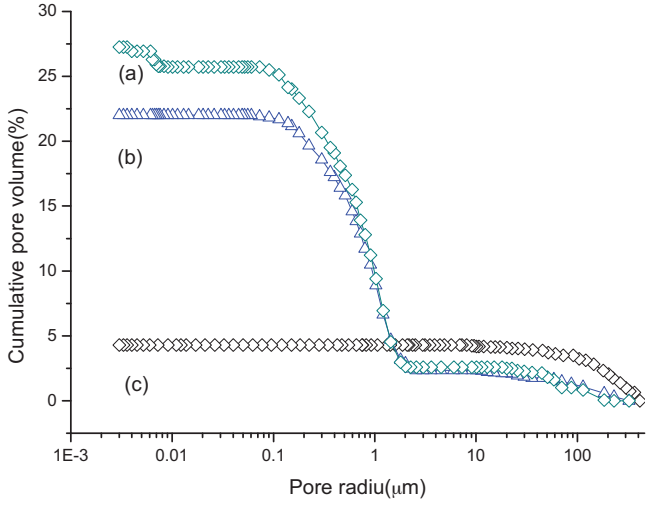

Fig. 7. The cumulative porosity distribution of the free-standing YSZ coatings: (a) as-sprayed; (b) heat-treated at 1250 °C for 10 h; (c) with CMAS and heat-treated at 1250 °C for 10 h.

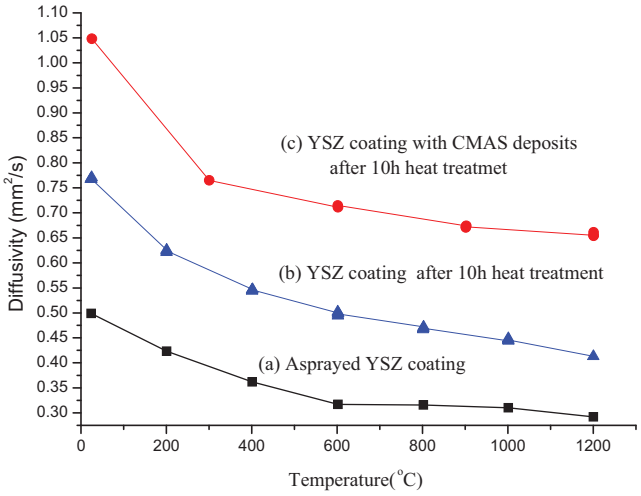

Fig. 8. Thermal difusivities of YSZ coatings: (a) as-sprayed; (b) heat-treated at 1250 °C for 10 h; (c) with CMAS and heat-treated at 1250 °C for 10 h.

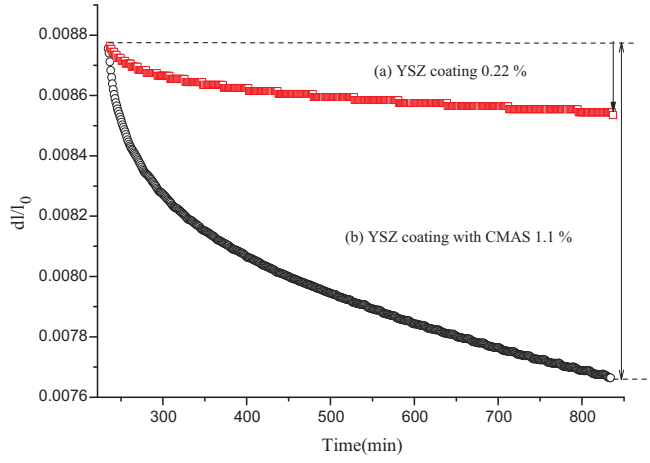

Fig. 9. . Sintering behavior of free-standing YSZ coating (a) and YSZ coating with CMAS (b) at 1250 °C for 10 h.

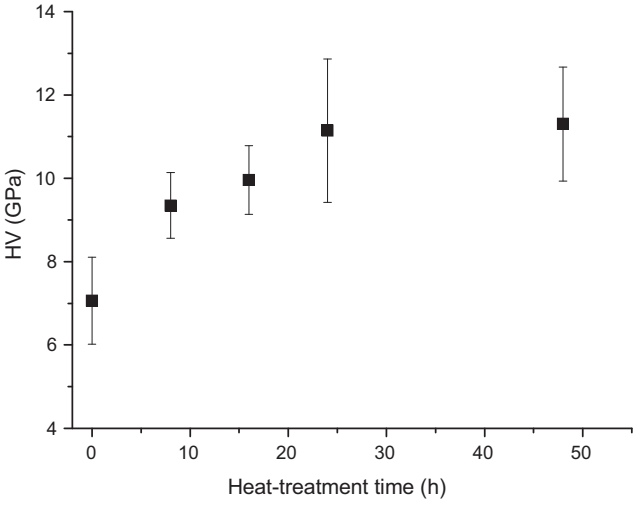

Fig. 10. Vickers micro-hardness for YSZ coatings with CMAS heat-treated at 1250 °C for different hours.

Therefore, it can be concluded that the CMAS penetration could compromise the thermal barrier capability of TBC.

There are hundreds of cooling channels in turbine blades, which are designed to reduce the surface temperature of blades in order to allow the blades to operate at high-temperatures. When thermal barrier coatings (especially for plasma sprayed coatings) are applied onto the blades, the surface chemical activity of the blades could be increased. In this case, CMAS deposits were prone to stick to the blade surfaces and block the cooling channels. As a result, the cooling effectiveness could be decreased and cause local over-heating of blade alloys. Simultaneously, for the TBC parts, due to degradation of thermal barrier effects, the temperature at the interface between the ceramic topcoat and bond coat rose up accordingly. Accelerated thickening of thermally grown oxide (TGO) could occur, which would lead to premature spallation of TBCs.

4.3. Failure analysis of YSZ coating with CMAS deposits

From above results, CMAS deposits melted at 1250 °C and rapidly infiltrated into the YSZ coating. At the interface between CMAS deposits and YSZ coating, the original t phase YSZ was dissolved and precipitated into finer particles of m-phase ZrO_2. As known, too much phase transformation of t-m would cause large volume expansion and deteriorate the integrity of TBC system, and eventually spallation failure of TBC.

On the other hand, the CMAS led to an accelerated sintering of YSZ coating. Sintering usually leads to shrinkage at the surface of a TBC. The sintering effect decreases gradually from the surface to the bond coat. This leads to an increase in Young's Modulus which decreases strain tolerance capability of the coating and increases top-coat stresses. The variation in the stress distribution also changes the strain energy release rate and failure mechanisms. This may be the mechanism by which the horizontal cracks form and the TBCs spall. In addition, for the case of those rotation blades, due to the increased thickness the CMAS layer deposition would increase the load of TBC system. This is also one of factors affecting service lifetime of TBCs.

5. Conclusions

The microstructure evolution and thermophysical properties of the plasma sprayed YSZ coatings attacked by CMAS at 1250 °C were investigated. The conclusions can be drawn as follows:

(1) Si and Ca in the CMAS rapidly penetrated the coating and accelerated sintering of the coating.
(2) At the interaction zone between the CMAS and YSZ coating, the YSZ coating was partially dissolved in the CMAS, inducing the phase transformation from tetragonal phase to monoclinic phase.
(3) Due to CMAS penetration, the porosity of the coating was reduced from ~25% to ~5%. As a result, the thermal diffusivity at 1200 °C increased from 0.3 mm^2/s to 0.7 mm^2/s, indicating a severe degradation in thermal barrier perfor-

mance. Also, the coating showed a more than 25% increase in the microhardness.

Acknowledgements

This research is sponsored by the New Century Excellent Talents in University (NCET), National Nature Science Foundations of China (NSFC, no. 50771009, no. 50731001 and no. 51071013) and National Basic Research Program (973 Program) of China under grant no. 2010CB631200.

References

1. Padture NP, Gell M, Jordan EH. Thermal barrier coatings for gas-turbine engine applications. *Science* 2002;**296**:280.
2. Stiger MJ, Yanar NM, Toppings MG, Pettit FS, Meier GHZ. Thermal barrier coatings for the 21st century. *Metallkd* 1999;**90**:1069.
3. Miller RA. Thermal barrier coatings for aircraft engines: history and directions. *J Therm Spray Technol* 1997;**1**:35.
4. Levi CG. Emerging materials and processes for thermal barrier systems. *Solid State Mater Sci* 2004;**1**:77.
5. Gleeson B. Thermal barrier coatings for aeroengine applications. *Propul Power* 2006;**22**:375.
6. Evans AG, Mumm DR, Hutchinson JW, Meier GH, Pettit FS. Mechanisms controlling the durability of thermal barrier coatings. *Prog Mater Sci* 2001;**46**:505.
7. Evans AG, He MY, Hutchinson JW. Mechanics-based scaling laws for the durability of thermal barrier coatings. *Prog Mater Sci* 2001;**46**:249.
8. Wellman RG, Nicholls JR. Some observations on erosion mechanisms of EB PVD TBCS. *Wear* 2000;**242**:89.
9. Wright PK, Evans AG. Mechanisms governing the performance of thermal barrier coatings. *Curr Opin Solid State Mater Sci* 1999;**4**:255.
10. Borom MP, Johnson CA, Peluso LA. Role of environmental deposits and operating surface temperature in spallation of air plasma sprayed thermal barrier coatings. *Surf Coat Technol* 1996;**86-87**:116.
11. Stott FH, Wet DJ, de Taylor R. Degradation of thermal-barrier coatings at very high temperatures. *MRS Bull* 1994;**10**:46.
12. Kim J, Dunn MG, Baran AJ, Wade DP, Tremba EL. Deposition of volcanic materials in the hot sections of two gas turbine engines. *J Eng Gas Turbines Power* 1993;**7**:641.
13. Smialek JL, Archer FA, Garlick RG. Turbine airfoil degradation in the Persian Gulf war. *JOM* 1994;**46**:39.
14. Mercer C, Faulhaber S, Evans AG, Darolia R. A delamination mechanism for thermal barrier coatings subject to calcium–magnesium–alumino–silicate (CMAS). *Acta Mater* 2005;**53**:1029.
15. Krämer S, Yang J, Levi CG, Johnson CA. Thermochemical interaction of thermal barrier coatings with molten CaO–MgO–Al_2O_3-SiO_2 (CMAS) deposits. *J Am Ceram Soc* 2006;**89**:3167.
16. Li L, Clarke DR. Effect of CMAS infiltration on radiative transport through an EB-PVD thermal barrier coating. *Int J Appl Ceram Technol* 2008;**5**:278.
17. Chen X. Calcium–magnesium–alumina–silicate (CMAS) delamination mechanisms in EB-PVD thermal barrier coatings. *Surf Coat Technol* 2006;**200**:3418.
18. Aygun A, Vasiliev AL, Padture NP. Novel thermal barrier coatings that are resistant to high-temperature attack by glassy deposits. *Acta Mater* 2007;**55**:6734.
19. Mohan P, Patterson T, Yao B, Sohn YH. Environmental degradation of thermal barrier coating and mitigation by electrophoretically deposited overlay. *J Therm Spray Technol* 2010;**1–2**:156.
20. Li L, Hitchman N, Knapp J. Failure of thermal barrier coatings subjected to CMAS attack. *J Therm Spray Technol* 2009;**1–2**:148.
21. Wu J, Guo HB, Zhou L, Wang L, Gong SK. Microstructure and thermal properties of plasma sprayed nanostructure YSZ thermal barrier coatings. *J Therm Spray Technol* 2010;**6**:1186.
22. Iwamotoa N, Umesakia N, Endo S. Characterization of plasma-sprayed zirconia coatings by X-ray diffraction and Raman spectroscopy. *Thin Solid Films* 1985;**1–2**(129):23.
23. Shaw TM, Duncombe PR. Forces between aluminum oxide grains in a silicate melt and their effect on grain boundary wetting. *J Am Ceram Soc* 1991;**74**:2495.
24. Jitcharoen J, Padture NP, Giannakopoulos AE, Suresh S. Hertzian-crack suppression in ceramics with elastic-modulus-graded surfaces. *J Am Ceram Soc* 1998;**49**:3255.
25. Lasse F, Lauri H, Takamichi I, Yoshifumi K, Yunie T. Experimental study of viscosities of selected CaO–MgO–Al_2O_3–SiO_2 slags and application of the Iida model. *Scand J Metall* 2003;**32**:273.
26. Guo HB, Murakami H, Kuroda S. Effect of hollow spherical powder size distribution on porosity and segmentation cracks in thermal barrier coatings. *J Am Ceram Soc* 2006;**89**:3797.
27. Guo HB, Kuroda S, Murakami H. Segmented thermal barrier coatings produced by atmospheric plasma spraying hollow powders. *Thin Solid Films* 2006;**506**:136.
28. Guo HB, Murakami H, Kuroda S. Effects of heat treatment on microstructures and physical properties of segmented thermal barrier coatings. *Mater Trans* 2005;**46**:1775.
29. Guo HB, Vaßen R, Stover D. Thermophysical properties and thermal cycling behavior of plasma sprayed thick thermal barrier coatings. *Surf Coat Technol* 2005;**192**:48.
30. Vaßen R, Czech N, Malléner W, Stamm W, Stöver D. Influence of impurity content and porosity of plasma-sprayed yttria-stabilized zirconia layers on the sintering behavior. *Surf Coat Technol* 2001;**141**:135.